Topological semimetal to insulator quantum phase transition in the Zintl compounds $Ba_2X(X = Si,Ge)$

Ziming Zhu,[1,2] Mingda Li,[3] and Ju Li[1,2,*]

[1]*Frontier Institute of Science and Technology, and State Key Laboratory for Mechanical Behavior of Materials, Xi'an Jiaotong University, 710054, Xi'an, People's Republic of China*

[2]*Department of Nuclear Science and Engineering and Department of Materials Science and Engineering, Massachusetts Institute of Technology, Cambridge, Massachusetts 02139, USA*

[3]*Department of Mechanical Engineering, Massachusetts Institute of Technology, Cambridge, Massachusetts 02139, USA*

(Received 23 April 2016; revised manuscript received 7 July 2016; published 13 October 2016)

By first-principles calculations, we find that $Ba_2X(X = Si,Ge)$ hosts a topological semimetal phase with one nodal ring in the $k_x = 0$ plane, which is protected by the glide mirror symmetry when spin-orbit coupling (SOC) is ignored. The corresponding drumheadlike surface flat band appears on the (100) surface in surface Green's function calculation. Furthermore, a topological-semimetal-to-insulator transition is found. The nodal line semimetal would evolve into a topological insulator as SOC is turned on. The topologically protected metallic surface states emerge around the $\overline{\Gamma}$ point, which could be tuned into the topologically trivial insulator state by more than 3% hydrostatic strain. These results reveal a category of materials showing quantum phase transition between topological semimetal and insulator, and tunability through elastic strain engineering.

DOI: 10.1103/PhysRevB.94.155121

I. INTRODUCTION

Topological insulators (TIs) [1,2] possess exotic metallic surface states but gapped bulk states. They have attracted enormous attention since the theoretical proposal of a two-dimensional (2D) TI in a HgTe/CdTe quantum well and three-dimensional (3D) TIs in the Bi_2Se_3 family of compounds [3–5], and experimental verifications thereafter [1,2,6]. The most striking characteristic of TI is the robust edge/surface state in a 2D/3D system, sheltered against backscattering from nonmagnetic impurities as long as the bulk gap remains open and the time-reversal symmetry is preserved [1–8]. Recently, it has been shown that the band topology could be extended into semimetallic systems where some band touches are exactly located at the Fermi level [9–16]. Based on the different band touches in the topological semimetal (TSM), a Dirac point, nodal line, or nodal ring would form on the Fermi surface as a consequence of nontrivial band crossing guaranteed by crystal symmetry and topology [11,12,17–23]. For instance, starting with two theoretical proposals in Na_3Bi and Cd_2As_3 [11,12], the TSM phase has been experimentally confirmed as an analog of 3D graphene for band structure with linear dispersion at different crystal planes [24,25]. In particular, Fermi arcs are expected to be detectable spectroscopically in TSM with the breaking of either time-reversal symmetry or inversion symmetry (Weyl semimetal), which have been verified in noncentrosymmetric TaAs-class materials [13,16,26,27].

Three-dimensional TSM could be driven into 3D TI with the breaking of rotational symmetry. For example, Zeng *et al.* found through first-principles calculations that rare earth monopnictide LaN is a TSM possessing a nodal ring when SOC is neglected, but exhibiting TI behavior when SOC is included [28]. Moreover, a nodal ring could be turned into a nodal point by SOC in the absence of inversion symmetry, dubbed the Weyl point [13,16]. The common feature between them is that the nodal ring from the crossing between the conduction band and the valence band is protected by the reflection symmetry and the time-reversal symmetry, and SOC plays a significant role in driving the quantum phase transition from TSM into TI. However, there is a lack of understanding on how SOC affects the nodal line state respecting the glide mirror symmetry. In this article, based on first-principles calculations, we find a TSM phase in $Ba_2X(X = Si,Ge)$ with a nodal ring in the $k_x = 0$ plane, which would evolve into the TI phase by SOC. Also, such TI could be further tuned into a normal semiconductor by hydrostatic strain (HSS). These investigations provide the evidence to understand the impact of SOC on the nodal line semimetal and strain-induced topological-semimetal-to-insulator transitions (TSMITs), and may also offer an avenue to search for alternative topological materials and quantum phase transitions.

II. CRYSTAL STRUCTURE AND METHODOLOGY

$Ba_2X(X = Si,Ge)$ belongs to the orthorhombic crystal system with the space group *Pnma* (No. 62). In this study, for brevity we take Ba_2Si as an example to introduce the electronic structures, as the similarity with Ba_2Ge is strong. The lattice constants are $a = 5.418$ Å, $b = 8.524$ Å, and $c = 10.174$ Å [29]. The corresponding primitive cell, shown in Fig. 1(a), consists of eight Ba and four Si. Ba contains two inequivalent $4c$ sites, Ba_1 (0.0185, 0.25, 0.6756) and Ba_2 (0.1513, 0.25, 0.083), whereas Si occupies the $4c$ site (0.251, 0.25, 0.4016). The bulk Brillouin zone (BZ) is illustrated in Fig. 1(b) along with the (100) BZ surface. The Vienna *ab initio* simulation package (VASP) was employed to calculate bulk band structure with the generalized gradient approximation (GGA) density functional and the projector augmented wave (PAW) method [30–32]. A Monkhorst-Pack **k** mesh of $11 \times 11 \times 11$ was used for the bulk calculation to sample the Brillouin zone and the energy cutoff for the plane-wave basis was set to 560 eV [33].

*liju@mit.edu

For convergence of electronic self-consistent calculations, a total energy difference criterion was defined as 10^{-8}eV. All atoms were fully relaxed in the internal coordinates until the total residual force was less than 10^{-3} eV/Å. To calculate the surface state, the d component of Ba and p of Si were obtained as the atomic orbital like Wannier functions for a tight-binding model as in Ref. [34]. The phonon spectrum was calculated using a supercell approach within the PHONON code [35].

III. RESULTS AND DISCUSSIONS

In the absence of SOC, band structure demonstrates the feature of the semimetal phase in bulk Ba_2Si as depicted in Fig. 1(c), where a band inversion happens along the $Y-\Gamma-Z$ direction, resulting in the nodal ring [36] from the crossing between the valence band and the conduction band that stays in the $k_x = 0$ plane [the inset of Fig. 1(c)]. The glide symmetry $G_x = M_x|(\frac{1}{2},0,0)$ is the combination of mirror reflection symmetry $M_x : (x,y,z) \to (-x,y,z)$ and a translation by a half lattice vector $\tau_x = (\frac{1}{2},0,0)$. Thus, the eigenvalue of G_x is the product of the eigenvalue of M_x and the phase factor induced by τ_x. The irreducible representations of the little group of **k** points in the $k_y - k_z$ plane are determined by the eigenvalue of M_x. As the Hamiltonian without SOC is spin-rotation invariant, i.e., $M_x^2 = 1$, the eigenvalue of M_x is $+1$ or -1 [Fig. 1(c)] [37]. According to this argument, two bands with different representations will not induce a band gap when they cross each other. Therefore, the appearance of the nodal ring in the absence of SOC is protected by the glide mirror symmetry. Taking SOC into consideration [Fig. 1(d)], two bands move away from each other and it is fully gapped along the whole high-symmetry direction. The opened gap is about 25 meV. This is identified as TSM-TI quantum phase transition (see below). From the comparisons of electronic structures with and without SOC, the variation of the whole band structure is rather small because the elements involved have light Z. It is worth mentioning that an inverted band order state already exists in the TSM phase as compared to the normal semiconductor phase, such as Sr_2Pb and Bi_2Te_3 [5,38] when SOC is turned off, although they would evolve into the TI phase in the presence of SOC. Additionally, the stability of Zintl compound Ba_2Si has been checked by computing the phonon dispersion as illustrated in Fig. 2, with no imaginary frequency along the high-symmetry line.

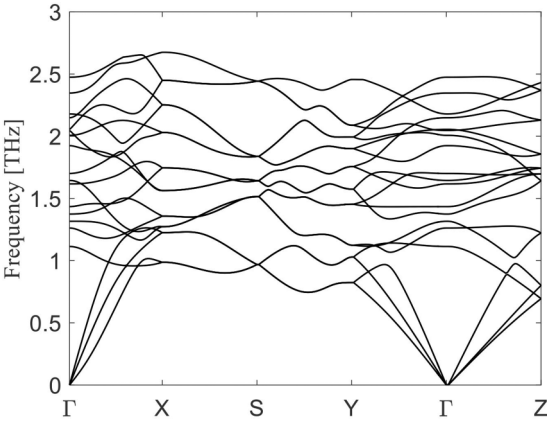

FIG. 2. Phonon dispersion in Ba_2Si along the high-symmetry directions.

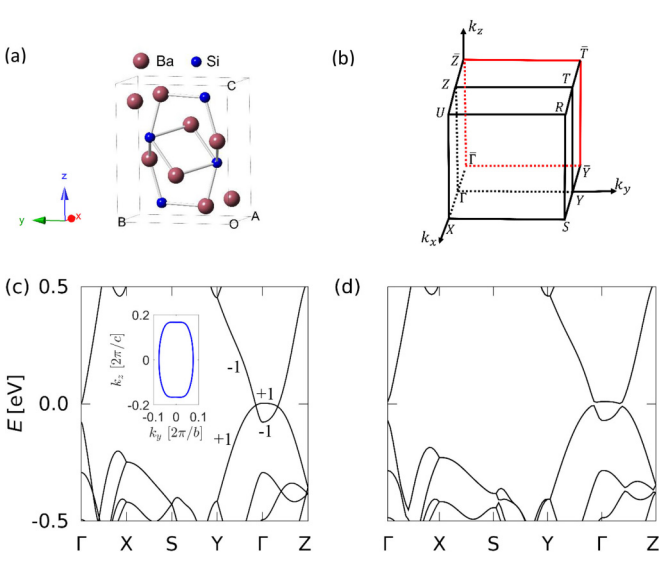

FIG. 1. (a) Side view of primitive unit cell of Ba_2Si along the x axis. (b) Three-dimensional bulk Brillouin zone and its projection onto the (100) surface, as well as high-symmetry points. Band structures from first-principles calculation (c) without and (d) with SOC. E_F is set to be zero in all panels. The number $+1$ or -1 labels the eigenvalue of the glide mirror plane ($k_x = 0$). The inset shows the nodal ring within the momentum space of $k_x = 0$.

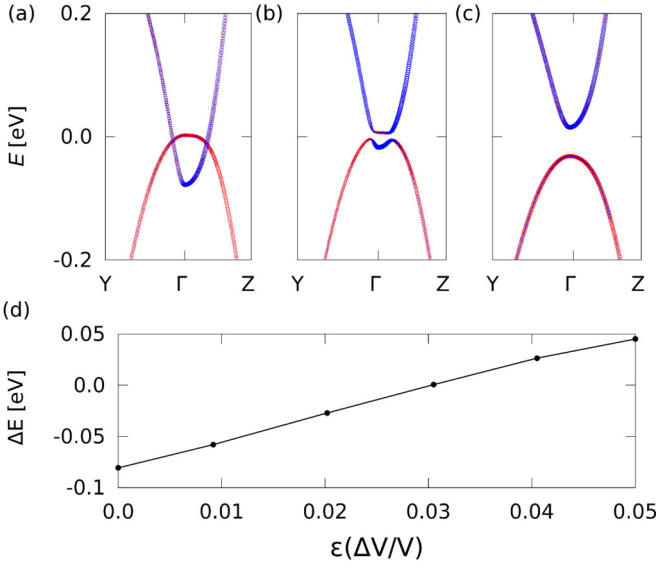

FIG. 3. The comparisons of the component in different atomic orbitals along the $Y-\Gamma-Z$ direction among (a) without SOC, (b) [(c)] zero strain (5% of HHS) with SOC, where the weight of atomic orbital Si(p) [Ba(d)] is proportional to the radius of the blue (red) circle. Band inversion could be seen clearly around the Γ point. (d) Energy difference between VBG and CBG (at the Γ point) vs HSS, $\varepsilon(\Delta V/V)$.

TABLE I. The parity of eight time-reversal invariant **k** points with SOC as discussed in Fig. 3 and their corresponding topological invariant.

	Γ	X	Y	Z	S	U	T	R	Z_2
SOC, HSS = 0%	−	+	+	+	+	+	+	+	1
SOC, HSS = 5%	+	+	+	+	+	+	+	+	0

Figures 3(a)–3(c) show the band-orbital characteristics around the Γ point to clarify the topological property, which has been analyzed from the wave functions of first-principles calculations. In the case of strain-free crystal, the valence band at the Γ point (VBG) is mainly composed of the Si(p) orbital, while the conduction band at the Γ point (CBG) consists of the Ba(d) orbital no matter whether SOC is introduced. With 5% of applied HSS, VBG and CBG exchange their atomic orbital with opposite band order, which obviously belongs to a topologically trivial semiconductor. Figure 3(d) illustrates that the energy difference between VBG and CBG decreases as a function of HSS, where topological phase transition occurs at about 3%. However, the energy gap between the valence band maximum and the conduction band minimum is almost unchanged as the strength of SOC does not rely much on strain. In reality, Ba_2Si possesses $p-d$ band inversion, instead of the p-s band inversion in the Sr_2Pb system though they share a similar crystal structure [38].

To confirm the topological nature of Ba_2Si in the case of small but finite SOC as discussed above, we followed the parity criteria proposed by Fu and Kane [39] for such an inversion symmetry system, i.e., calculating the product of the parity of Bloch wave function for the occupied band at the time-reversal invariant momenta (TRIM) in the first Brillouin zone. There are seven TRIMs with "+" of the parity at X,Y,Z,S,U,T, and R, whereas the parity of the Γ point depends on whether band inversion occurs as listed in Table I. For zero-strain case, the topological invariant Z_2 is 1. Furthermore, HSS effect could induce a transition from TI into topologically trivial semiconductor, providing the possibility to study the tunability of topological phase in the Ba_2Si system.

To further investigate the nontrivial surface state, we performed calculation of the projected band structure in semi-infinite Ba_2Si onto the (100) surface, by using the iterative Green's function method [40] implemented in the WANNIER_TOOLS package [41] from a tight-binding model with Wannier function constructed from plane-wave solutions. Figure 4(a) illustrates that a drumheadlike surface flat band emerges around the Fermi level connecting two crossing

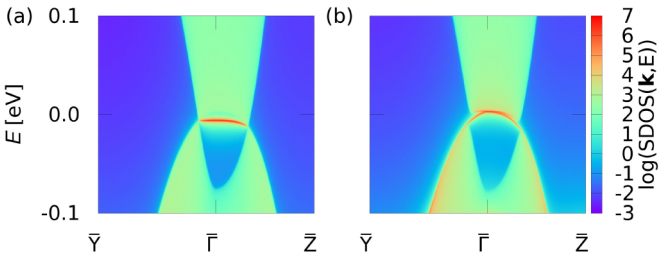

FIG. 4. Surface density of states (SDOS) in Ba_2Si (a) without and (b) with SOC. The red lines highlight the topologically protected metallic surface states along $\bar{Y}-\bar{\Gamma}-\bar{Z}$.

points, which actually will form a drumheadlike Fermi surface. It should be pointed out that this type of flat band might be the key for high-temperature superconductivity [42]. Taking SOC into account, one could see that there is a metallic surface state around the $\bar{\Gamma}$ point, coinciding with the previous calculation of Z_2. In Ba_2Si the topologically protected surface state appears on the (100) surface, distinct from that of Sr_2Pb on the (010) surface stemming from the distinct band inversion [38] structure. As the SOC strength may diminish with a lighter element, the surface density of states (SDOS) of a quasi nodal line may reappear when replacing Ba by Mg or Ca [22].

In summary, we report the quantum phase transition in Ba_2Si from nodal line semimetal into topological insulator as a result of SOC based on first-principles calculation. The nodal line could still survive in the glide mirror symmetry system without including SOC, but would be fully gapped when SOC is introduced. Using Green's function calculation, we find that the nodal line semimetal demonstrates the drumheadlike surface flat band around the Fermi level, which turns into the metallic surface state with SOC. Our work also shows that such topological phase could totally disappear by applying more than 3% of HSS.

ACKNOWLEDGMENTS

We thank L. Fu, J. W. Liu, and Q. S. Wu for helpful conversations. We would like to thank Q. S. Wu for helping calculate the eigenvalue of the glide mirror symmetry. This work is supported by National Basic Research Program of China, under Contract No. 2012CB619402, and a grant-in-aid of 985 Project from Xi'an Jiaotong University. J.L. acknowledges support by NSF DMR-1410636. M.L. would like to acknowledge the support from S3TEC, an EFRC funded by DOE BES under Award No. DE-SC0001299/DE-FG02-09ER46577.

The authors declare no competing financial interests.

[1] M. Z. Hasan and C. L. Kane, Colloquium: Topological insulators, Rev. Mod. Phys. **82**, 3045 (2010).

[2] X.-L. Qi and S.-C. Zhang, Topological insulators and superconductors, Rev. Mod. Phys. **83**, 1057 (2011).

[3] B. A. Bernevig, T. L. Hughes, and S.-C. Zhang, Quantum spin Hall effect and topological phase transition in HgTe quantum wells, Science **314**, 1757 (2006).

[4] C. L. Kane and E. J. Mele, Quantum Spin Hall Effect in Graphene, Phys. Rev. Lett. **95**, 226801 (2005).

[5] H. Zhang, C.-X. Liu, X.-L. Qi, X. Dai, Z. Fang, and S.-C. Zhang, Topological insulators in Bi_2Se_3, Bi_2Te_3 and Sb_2Te_3 with a single Dirac cone on the surface, Nat. Phys. **5**, 438 (2009).

[6] M. König, S. Wiedmann, C. Brüne, A. Roth, H. Buhmann, L. W. Molenkamp, X.-L. Qi, and S.-C. Zhang, Quantum spin

Hall insulator state in HgTe quantum wells, Science **318**, 766 (2007).

[7] J. Moore, Topological insulators: The next generation, Nat. Phys. **5**, 378 (2009).

[8] X.-L. Qi and S.-C. Zhang, The quantum spin Hall effect and topological insulators, Phys. Today **63**, 33 (2010).

[9] Y. Kim, B. J. Wieder, C. L. Kane, and A. M. Rappe, Dirac Line Nodes in Inversion-Symmetric Crystals, Phys. Rev. Lett. **115**, 036806 (2015).

[10] X. Wan, A. M. Turner, A. Vishwanath, and S. Y. Savrasov, Topological semimetal and Fermi-arc surface states in the electronic structure of pyrochlore iridates, Phys. Rev. B **83**, 205101 (2011).

[11] Z. Wang, Y. Sun, X.-Q. Chen, C. Franchini, G. Xu, H. Weng, X. Dai, and Z. Fang, Dirac semimetal and topological phase transitions in $A_3Bi(A = Na,K,Rb)$, Phys. Rev. B **85**, 195320 (2012).

[12] Z. Wang, H. Weng, Q. Wu, X. Dai, and Z. Fang, Three-dimensional Dirac semimetal and quantum transport in Cd_3As_2, Phys. Rev. B **88**, 125427 (2013).

[13] H. Weng, C. Fang, Z. Fang, B. A. Bernevig, and X. Dai, Weyl Semimetal Phase in Noncentrosymmetric Transition-Metal Monophosphides, Phys. Rev. X **5**, 011029 (2015).

[14] L. S. Xie, L. M. Schoop, E. M. Seibel, Q. D. Gibson, W. Xie, and R. J. Cava, Potential ring of Dirac nodes in a new polymorph of Ca_3P_2, APL Mat. **3**, 083602 (2015).

[15] R. Yu, H. Weng, Z. Fang, X. Dai, and X. Hu, Topological Node-Line Semimetal and Dirac Semimetal State in Antiperovskite Cu_3PdN, Phys. Rev. Lett. **115**, 036807 (2015).

[16] S.-M. Huang, S.-Y. Xu, I. Belopolski, C.-C. Lee, G. Chang, B. Wang, N. Alidoust, G. Bian, M. Neupane, C. Zhang, S. Jia, A. Bansil, H. Lin, and M. Zahid Hasan, A Weyl Fermion semimetal with surface Fermi arcs in the transition metal monopnictide TaAs class, Nat. Commun. **6**, 7373 (2015).

[17] G. Mikitik and Y. V. Sharlai, Band-contact lines in the electron energy spectrum of graphite, Phys. Rev. B **73**, 235112 (2006).

[18] H. Weng, Y. Liang, Q. Xu, R. Yu, Z. Fang, X. Dai, and Y. Kawazoe, Topological node-line semimetal in three-dimensional graphene networks, Phys. Rev. B **92**, 045108 (2015).

[19] G. Bian *et al.*, Topological nodal-line fermions in spin-orbit metal $PbTaSe_2$, Nat. Commun. **7**, 10556 (2016).

[20] G. Bian, T.-R. Chang, H. Zheng, S. Velury, S.-Y. Xu, T. Neupert, C.-K. Chiu, S.-M. Huang, D. S. Sanchez, I. Belopolski, N. Alidoust, P.-J. Chen, G. Chang, A. Bansil, H.-T. Jeng, H. Lin, and M. Zahid Hasan, Drumhead surface states and topological nodal-line fermions in $TlTaSe_2$, Phys. Rev. B **93**, 121113 (2016).

[21] A. Yamakage, Y. Yamakawa, Y. Tanaka, and Y. Okamoto, Line-node Dirac semimetal and topological insulating phase in noncentrosymmetric pnictides $CaAgX(X = P,As)$, J. Phys. Soc. Jpn. **85**, 013708 (2015).

[22] H. Huang, J. Liu, D. Vanderbilt, and W. Duan, Topological nodal-line semimetals in alkaline-earth stannides, germanides, and silicides, Phys. Rev. B **93**, 201114 (2016).

[23] Y.-H. Chan, C.-K. Chiu, M. Y. Chou, and A. P. Schnyder, Ca_3P_2 and other topological semimetals with line nodes and drumhead surface states, Phys. Rev. B **93**, 205132 (2016).

[24] Z. Liu, B. Zhou, Y. Zhang, Z. J. Wang, H. M. Weng, D. Prabhakaran, S. K. Mo, Z. X. Shen, Z. Fang, X. Dai, Z. Hussain, and Y. L. Chen, Discovery of a three-dimensional topological Dirac semimetal, Na_3Bi, Science **343**, 864 (2014).

[25] M. Neupane, S.-Y. Xu, R. Sankar, N. Alidoust, G. Bian, Chang Liu, Ilya Belopolski, T.-R. Chang, H.-T. Jeng, H. Lin, A. Bansil, F. Chou, and M. Zahid Hasan, Observation of a three-dimensional topological Dirac semimetal phase in high-mobility Cd_3As_2, Nat. Commun. **5**, 3786 (2014).

[26] S.-Y. Xu *et al.*, Discovery of a Weyl fermion semimetal and topological Fermi arcs, Science **349**, 613 (2015).

[27] B. Lv, H. M. Weng, B. B. Fu, X. P. Wang, H. Miao, J. Ma, P. Richard, X. C. Huang, L. X. Zhao, G. F. Chen, Z. Fang, X. Dai, T. Qian, and H. Ding, Experimental Discovery of Weyl Semimetal TaAs, Phys. Rev. X **5**, 031013 (2015).

[28] M. Zeng *et al.*, Topological semimetals and topological insulators in rare earth monopnictides, arXiv:1504.03492v1 [cond-mat.mes-hall].

[29] A. Jain, S. P. Ong, G. Hautier, W. Chen, W. D. Richards, S. Dacek, S. Cholia, D. Gunter, D. Skinner, G. Ceder, and K. A. Persson, Commentary: The Materials Project: A materials genome approach to accelerating materials innovation, APL Mater. **1**, 011002 (2013).

[30] G. Kresse and J. Furthmüller, Efficiency of ab-initio total energy calculations for metals and semiconductors using a plane-wave basis set, Comput. Mater. Sci. **6**, 15 (1996).

[31] G. Kresse and J. Hafner, *Ab initio* molecular dynamics for open-shell transition metals, Phys. Rev. B **48**, 13115 (1993).

[32] M. C. Payne, M. P. Teter, D. C. Allan, T. A. Arias, and J. D. Joannopoulos, Iterative minimization techniques for ab initio total-energy calculations: Molecular dynamics and conjugate gradients, Rev. Mod. Phys. **64**, 1045 (1992).

[33] H. J. Monkhorst and J. D. Pack, Special points for Brillouin-zone integrations, Phys. Rev. B **13**, 5188 (1976).

[34] A. A. Mostofi, J. R. Yates, Y.-S. Lee, I. Souza, D. Vanderbilt, and N. Marzari, Wannier90: A tool for obtaining maximally-localised Wannier functions, Comput. Phys. Commun. **178**, 685 (2008).

[35] X. Gonze and C. Lee, Dynamical matrices, Born effective charges, dielectric permittivity tensors, and interatomic force constants from density-functional perturbation theory, Phys. Rev. B **55**, 10355 (1997).

[36] T. Bzdušek, Q. Wu, A. Rüegg, M. Sigrist, and A. A. Soluyanov, Nodal-chain metals, Nature (London) **538**, 75 (2016).

[37] C. Fang and L. Fu, New classes of three-dimensional topological crystalline insulators: Nonsymmorphic and magnetic, Phys. Rev. B **91**, 161105 (2015).

[38] Y. Sun, X.-Q. Chen, C. Franchini, D. Li, S. Yunoki, Y. Li, and Z. Fang, Strain-driven onset of nontrivial topological insulating states in Zintl Sr_2X compounds $(X = Pb,Sn)$, Phys. Rev. B **84**, 165127 (2011).

[39] L. Fu and C. L. Kane, Topological insulators with inversion symmetry, Phys. Rev. B **76**, 045302 (2007).

[40] M. P. Lopez Sancho, J. M. Lopez Sancho, J. M. L. Sancho, and J. Rubio, Highly convergent schemes for the calculation of bulk and surface Green functions, J. Phys. F: Met. Phys. **15**, 851 (1985).

[41] Q. S. Wu, https://github.com/quanshengwu/wannier_tools (2015).

[42] N. Kopnin, T. Heikkilä, and G. Volovik, High-temperature surface superconductivity in topological flat-band systems, Phys. Rev. B **83**, 220503 (2011).